pubs.acs.org/acschemicalbiology

Articles

Cell Morphological Profiling Enables High-Throughput Screening for PROteolysis TArgeting Chimera (PROTAC) Phenotypic Signature

Maria-Anna Trapotsi, Elizabeth Mouchet, Guy Williams, Tiziana Monteverde, Karolina Juhani, Riku Turkki, Filip Miljković, Anton Martinsson, Lewis Mervin, Kenneth R. Pryde, Erik Müllers, Ian Barrett, Ola Engkvist, Andreas Bender, and Kevin Moreau*

Cite This: *ACS Chem. Biol.* 2022, 17, 1733–1744

Read Online

ACCESS | Metrics & More | Article Recommendations | Supporting Information

ABSTRACT: PROteolysis TArgeting Chimeras (PROTACs) use the ubiquitin−proteasome system to degrade a protein of interest for therapeutic benefit. Advances made in targeted protein degradation technology have been remarkable, with several molecules having moved into clinical studies. However, robust routes to assess and better understand the safety risks of PROTACs need to be identified, which is an essential step toward delivering efficacious and safe compounds to patients. In this work, we used Cell Painting, an unbiased high-content imaging method, to identify phenotypic signatures of PROTACs. Chemical clustering and model prediction allowed the identification of a mitotoxicity signature that could not be expected by screening the individual PROTAC components. The data highlighted the benefit of unbiased phenotypic methods for identifying toxic signatures and the potential to impact drug design.

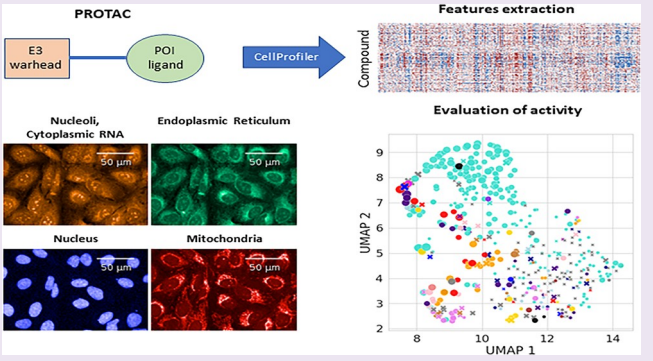

INTRODUCTION

PROteolysis TArgeting Chimeras (PROTACs) belong to a category of compounds also referred to as beyond the Rule-of-5 (bRo5) as they do not comply with Lipinski's Rule-of-5 (Ro5). The prediction and/or better understanding of the consequences for drug screening are limited by the lack of descriptors and methodologies for robust safety profiling. Hence, there is a need for descriptors tailored for or that are "compatible" with the bRo5 new data modalities.[1,2] There have been machine learning approaches for the prediction of drug toxicity using physiochemical descriptors, structural alerts, and high-throughput imaging data for small molecules.[3−5] However, computational prediction for new modalities has been less investigated. As a new therapeutic modality, PROTACs are raising multiple concerns on various aspects such as safety, ADME properties, toxicity, and others.[6] A potential approach to profile PROTACs and improve understanding of their safety aspects could be the use of high-throughput imaging (HTI) assays, which have become easier to run over the recent years. HTI assays have been useful in the better understanding of a compound's mode of action,[7−12] but from a practical angle, they have also been used to predict a wide range of efficacy and safety factors.[13−16] One of the assays that is currently used by academic groups and pharmaceutical companies is the Cell Painting assay.[7,9,13,17] Phenotypes from this assay are not obtained with any particular biological point of interest in mind and can be considered as image-based fingerprints of a compound covering a wide range of information.[7,18,19]

Here, we report for the first time that the Cell Painting assay can be used as a high-throughput imaging assay to profile morphological changes induced by PROTACs. Cell Painting descriptors proved to be sufficient to train models with good predictive performance. We proved that these profiles can be useful in mitochondrial toxicity prediction of PROTACs, highlighting that image-based data can be used in both supervised and unsupervised machine learning approaches and provide information for the safety assessment of compounds such as mitochondrial toxicity, which has been related to attrition of drugs and late-stage market withdrawals.[20]

RESULTS AND DISCUSSION

Morphological Profiling Detected PROTAC Activity. A total of 341 PROTACs and 149 non-PROTACs, directed at more than 15 different targets, were profiled with the Cell Painting assay in U-2 OS cells. PROTACs are bivalent molecules that use the natural function of E3 ligases to

Received: January 25, 2022
Accepted: May 31, 2022
Published: July 6, 2022

https://doi.org/10.1021/acschembio.2c00076
ACS Chem. Biol. 2022, 17, 1733−1744

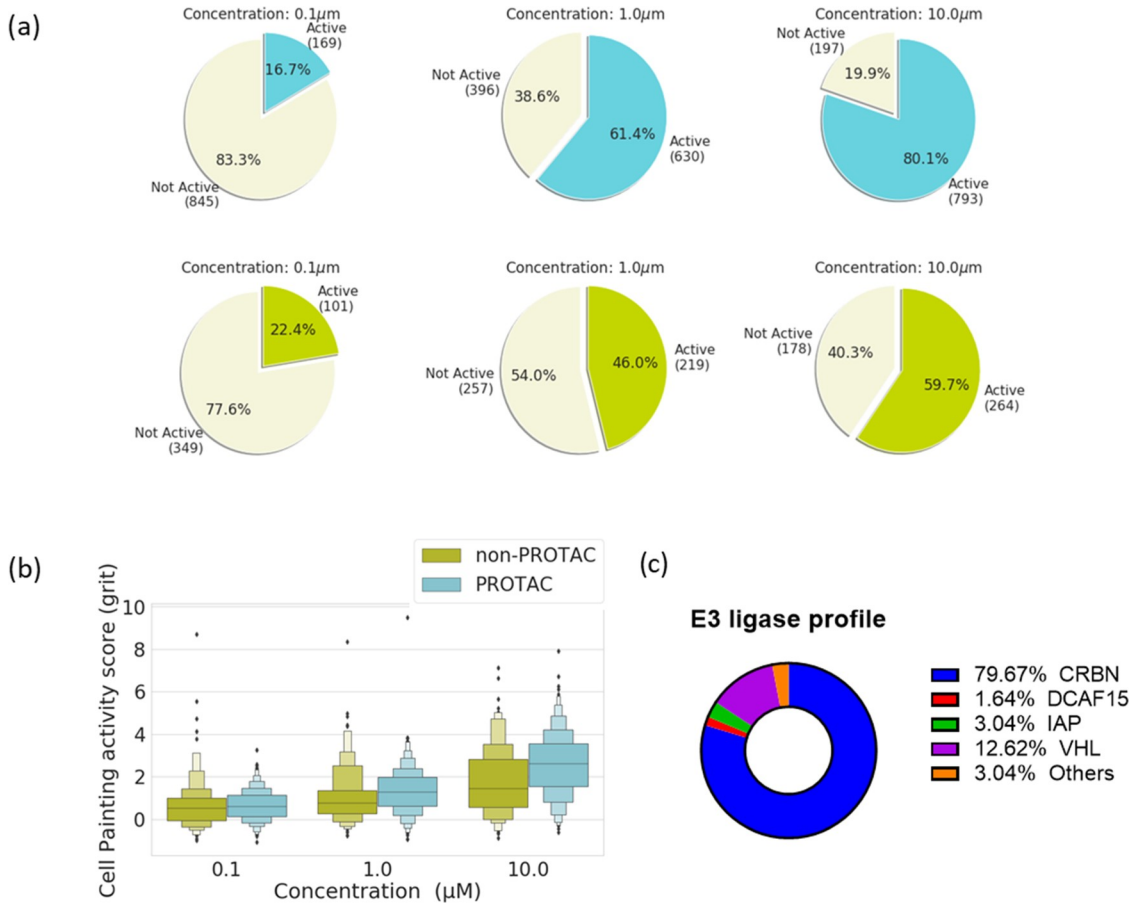

Figure 1. Cell Painting activity score for PROTAC and non-PROTAC compounds. (a) Percentage of PROTAC and non-PROTAC compounds identified as active on the Cell Painting assay with the Euclidean-based method (i.e., compounds that are able to change the cellular morphology) at concentrations of 0.1, 1, and 10 μM. The Euclidean distance-based method showed that the number of active compounds increases as the concentration increases. (b) Cell Painting activity score in the form of the grit score across all concentrations (0.1, 1, and 10 μM). Both PROTAC and non-PROTAC compounds' activity on the Cell Painting assay (in the form of the grit score) increased as the concentration increased. (c) Classification of the PROTAC molecules based on the E3 ligase used.

ubiquitinate a target protein for degradation through the proteasome. The non-PROTAC compounds include small-molecule compounds, which are inhibitors of the targets that PROTACs are degrading, E3 ligase ligands, and reference compounds that have shown mitochondrial toxicity. Following the compounds' profiling with the Cell Painting assay, morphological features were calculated with a CellProfiler. Morphological features were normalized, and a feature selection process was applied. In the final step, the activity of PROTACs on the Cell Painting assay was evaluated and PROTACs-Cell Painting features were used as descriptors for training the *in silico* mitotoxicity models.

PROTAC profiles together with non-PROTAC molecules were used to understand whether they show systematically different Cell Profiling readouts compared to neutral controls, based on two metrics: Euclidean distance-based and grit score activity metric. The results from the Euclidean distance-based method showed that out of the ∼1000 (three replicates per PROTAC) profiles obtained from testing PROTACs at concentrations 0.1, 1, and 10 μM, 17, 61, and 80% of the profiles, respectively, displayed cellular morphology different from the neutral controls (Figure 1a). In line, higher grit scores were observed with increasing concentrations (median ± standard deviations of 0.65 ± 0.72, 1.32 ± 1.07, and 2.56 ± 1.49 for concentrations of 0.1, 1, and 10 μM, respectively; Figure 1b). The main E3 ligases used by PROTACs are CRBN and VHL, and the vast majority of the compounds profiled with Cell Painting were using those two E3 ligases (Figure 1c). However, compounds using other E3 ligases such as DCAF15 or IAP were also included (Figure 1c). For non-PROTAC compounds, similar trends were observed, where 22, 46, and 60% of a total of ∼450 profiles displayed cellular morphology different from the controls (Figure 1a). Similarly, higher grit scores were observed with increasing concentrations (median ± standard deviations of 0.65 ± 1.20, 1.04 ± 1.30, and 1.80 ± 1.60 for concentrations of 0.1, 1, and 10 μM, respectively; Figure 1b). Hence, we observed a clear dose−response relationship in the data set examined here. The activity in the Cell Painting assay increased with concentration, but 17% of the PROTAC and 22% of the non-PROTAC profiles showed activity at 0.1 μM. We further evaluated how similar are the profiles between concentrations for each PROTAC. The mean Pearson correlations were equal to 0.26, 0.21, and 0.33 for comparisons between 0.1 vs 1, 0.1 vs 10, and 1 vs 10 μM, respectively. There is a degree of similarity between concentrations 1 and 10 μM, but a lower correlation was observed for 0.1 μM against the higher concentrations (1 and 10 μM), as shown in Figure S2a,b.

Looking at particular examples, we focused on a commercially available PROTAC data set, which included

https://doi.org/10.1021/acschembio.2c00076
ACS Chem. Biol. 2022, 17, 1733−1744

PROTACs targeting BRD4 and PROTACs targeting CDK proteins (Table 1, Figures 2 and S3). All previously published

Table 1. Cell Painting Activity Score (Grit) for Published PROTACs

		grit score at different concentrations (μM)		
compound name	target	0.1	1	10
MZ1	BRD4	1.60	3.84	dead cells
ZXH 3−26	BRD4	0.92	2.19	4.31
AT1	BRD4	1.22	2.15	4.20
dBET1	BRD4	−0.47	1.27	2.34
BSJ-03-123	CDK6	0.81	2.78	2.17
BSJ-03-204	CDK4/6	1.17	2.39	1.69
BSJ-04-132	CDK4	0.91	1.20	1.82
CM11	VHL	0.92	0.15	1.95
CRBN-6-5-5-VHL	CRBN	1.03	2.04	2.63
THAL-SNS-032	CDK9	−0.69	2.59	5.42
TL 13-12	ALK	2.08	1.50	5.46
lenalidomide	IKZF1, IKZF3	0.56	0.32	−0.18
pomalidomide	IKZF1, IKZF3	0.46	0.45	−0.02

PROTACs showed activity in the Cell Painting assay, including PROTACs targeting BRD4 and PROTACs targeting the cell-cycle regulators CDK proteins (Figure 2). Among the BRD4 PROTACs, MZ1 and ZXH 3−26 were the most active PROTAC compounds, while dBET1 was the least active (Figure 2), matching the degradation potency described for these compounds at BRD4 degradation, suggesting that the activity seen is an on-target effect. Among the CDK degraders, the PROTAC targeting CDK9 (THAL-SNS-032) was the most active. This makes it a pharmacologically interesting PROTAC because of its selective degradation of CDK9 with limited effects on the protein level of other CDKs.[21] In addition, THAL-SNS-032 has shown a prolonged pharmacodynamic effect compared with traditional kinase inhibitors.[21] Looking at the raw images, it was clear that the CDK9 degrader caused a reduction in nucleoli formation, suggesting a cell-cycle arrest effect, in line with the function of CDK9 in cell-cycle progression (Figure 2). This phenotype is plausible given that CDK9 inhibitors—such as the Flavopiridol—promote nucleolar disintegration by inhibiting early rRNA processing and transcription.[22]

Cell Painting Projection Revealed Different PROTAC Signatures. Next, a dimensionality reduction of the PROTACs-Cell Painting profiles was performed with uniform manifold approximation and projection (UMAP)[23] to understand which phenotypic responses are clustered together using Cell Profiling readouts with this method. The results of this analysis are shown in Figure 3, which suggested a range of different, distinguishable Cell Painting signatures for PROTACs targeting various targets (Figure 3). Furthermore, chemical clustering varied with the concentration of PROTACs used and the Cell Painting activity score (1 vs 10 μM; Figure 3). Looking at specific compounds targeting BRD4, the small-molecule inhibitor MS402 clustered together with BRD4 targeting PROTACs, suggesting a similar mode of action (Figure 3, orange annotation). Interestingly, PROTACs from different projects clustered to different regions, suggesting a different mode of action (Figure 3). Considering only the grit score, we did not observe a strong correlation with the primary pharmacology (target degradation; Figure S3a) and clearly observed some Cell Painting activity even when the primary target was not expressed in U-2 OS or when the compound showed poor degradation activity (Figure S3a). This was particularly evident for compounds from Targets 9, 11, and 14 where PROTACs with no degradation activity were still showing a high grit score (Figure S3b). These data suggest that the grit score is only one part of the Cell Painting data analysis and other parameters need to be used to capture the full signal from compounds such as feature extraction like we did for the degrader THAL-SNS-032, which clearly showed on-target activity via the loss of nucleoli (Figure 2). However, the observation of a poor correlation between primary pharmacology and the grit score led us to investigate whether we could link the Cell Painting signature of these PROTACs to a safety finding.

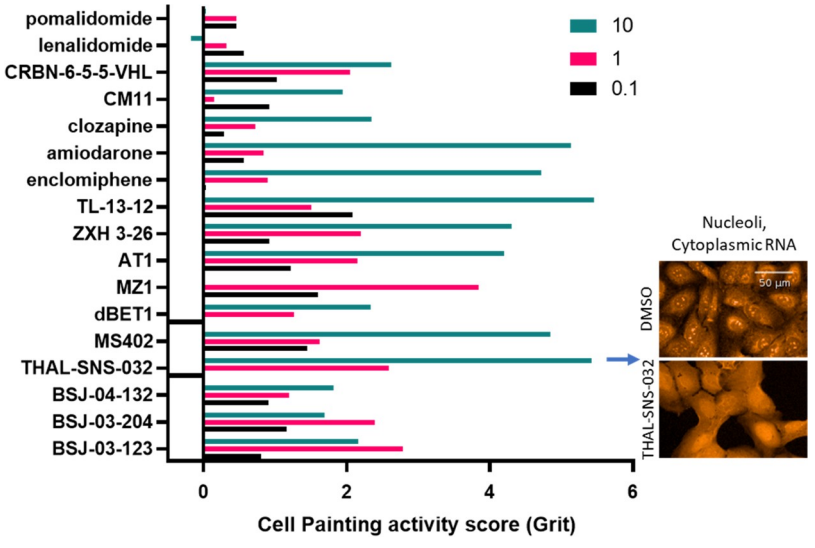

Figure 2. Cell Painting activity score (grit) for published PROTAC and non-PROTAC compounds. The published non-PROTAC compounds' data set consists of commonly used compounds as E3 ligand parts for PROTACs and three approved drugs (amiodarone, clozapine, and acetaminophen).

https://doi.org/10.1021/acschembio.2c00076
ACS Chem. Biol. 2022, 17, 1733−1744

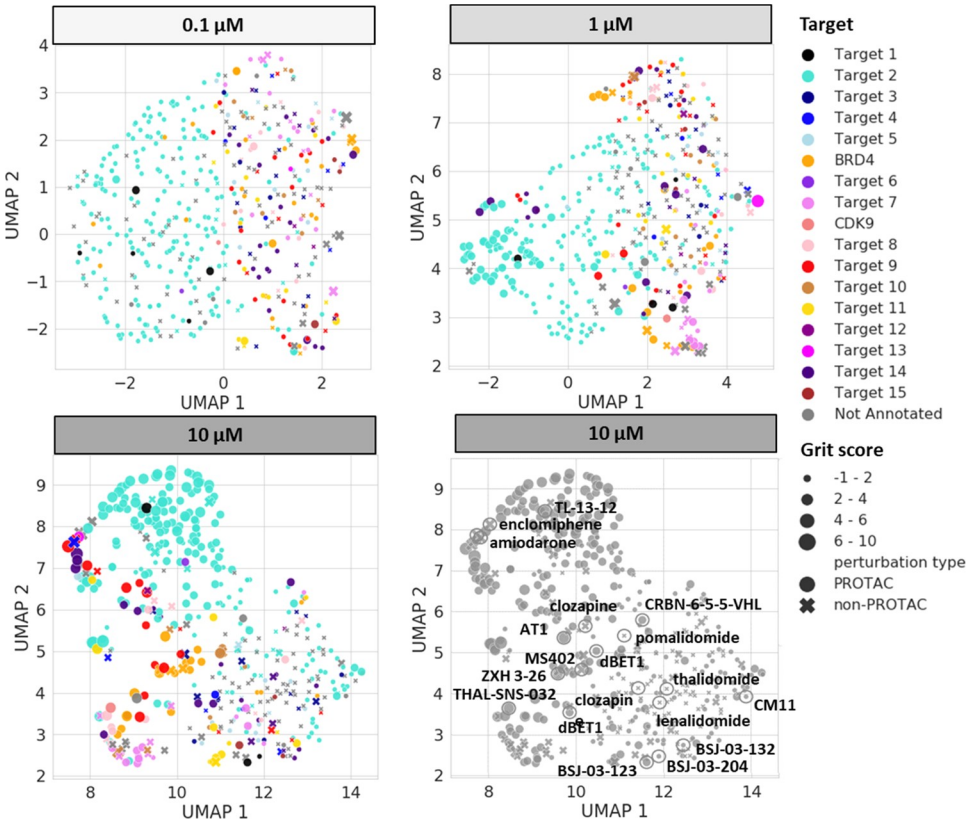

Figure 3. Uniform manifold approximation (UMAP) analysis. UMAP coordinates at concentrations 0.1, 1, and 10 μM of all perturbations labeled with the protein that is inhibited or degraded by each non-PROTAC or PROTAC compound, respectively. Published PROTAC or non-PROTAC compounds are annotated in the UMAP plot for 10 μM.

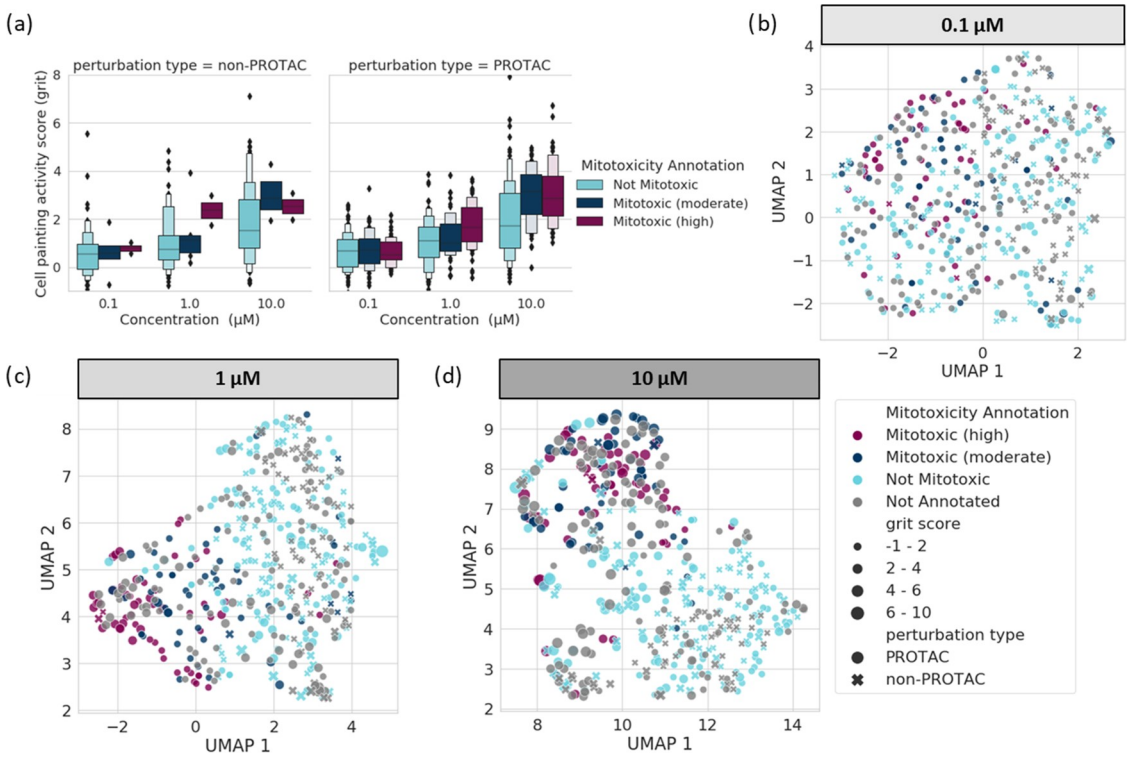

Figure 4. Cell Painting activity with the mitochondrial toxicity assay endpoint. (a) Cell Painting activity score in the form of grit score across concentrations 0.1, 1.0, and 10.0 μM and labeled based on a mitochondrial toxicity assay endpoint. Uniform manifold approximation (UMAP) coordinates of all perturbations labeled with mitotoxicity annotations at concentrations (b) 0.1, (c) 1, and (d) 10 μM.

https://doi.org/10.1021/acschembio.2c00076
ACS Chem. Biol. 2022, 17, 1733−1744

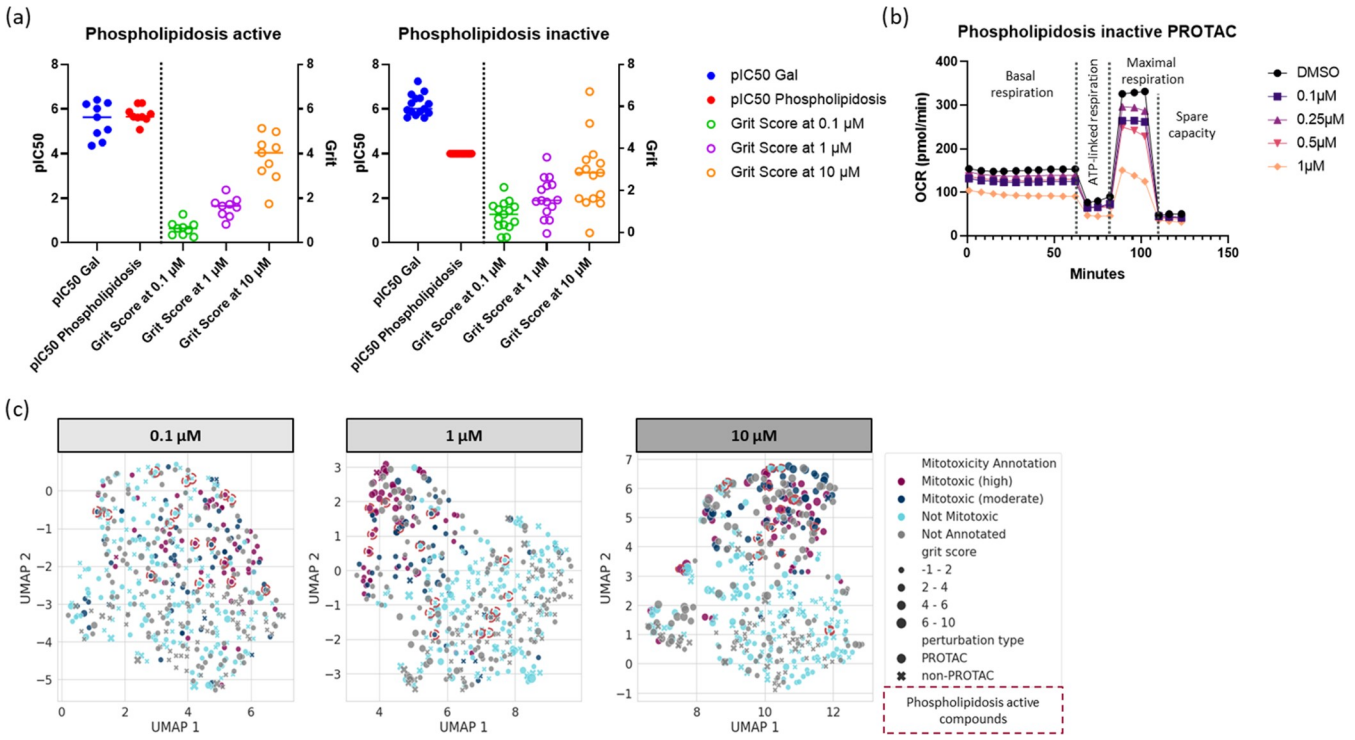

Figure 5. Phospholipidosis assessment of mitochondrial toxicity. (a) Classification of phospholipidosis active and inactive compounds together with Galactose pIC_{50} and the grit scores at 0.1, 1, and 10 μM. (b) Mitochondrial respiration measurement using the Seahorse assay. (c) Uniform manifold approximation (UMAP) coordinates of all perturbations labeled with mitotoxicity and phospholipidosis annotations at concentrations 0.1, 1, and 10 μM.

Cell Painting Signatures Were Able to Detect Activity on Mitochondria. To investigate whether Cell Painting profiles could be used to evaluate specific PROTAC safety liabilities, we employed annotations of *in vitro* mitotoxicity that were available for part of our compound set. Mitochondrial toxicity annotations for the PROTAC and non-PROTAC compounds were extracted from the Glu/Gal assay.[24] In this assay, cells are grown in two different media: a high-glucose and a galactose media. Cells grown in a high-glucose-containing medium use glycolysis for adenosine triphosphate (ATP) generation and are resistant to mitochondrial insult. Cells grown in a galactose-containing medium rely almost exclusively on mitochondria for their ATP production and, hence, are very sensitive to mitochondrial insult.[24] In total, 221 compounds, where 96 were annotated active (mitotoxic) and 125 inactive (not mitotoxic), were used to train the models. Out of the 221 compounds, 149 were PROTACs with 90 having been annotated mitotoxic and 59 having been annotated not mitotoxic. The annotations were further categorized as highly mitotoxic (IC_{50} < 1 μM; 51 compounds), moderately mitotoxic (IC_{50} between 1 and 10 μM; 44 compounds), and not mitotoxic (IC_{50} > 10 μM; 126 compounds). At a concentration of 10 μM, the mean grit scores were 3.01 ± 1.31, 3.09 ± 1.20, and 1.98 ± 1.59 for highly, moderately, and not-mitotoxic PROTACs, respectively (Figure 4a). At a concentration of 1 μM, the mean grit scores were 1.75 ± 0.97, 1.24 ± 0.91, and 1.14 ± 1.28 for highly, moderately, and not-mitotoxic PROTACs, respectively. The same trend was not observed at concentration 0.1 μM, where the mean grit scores were 0.64 ± 0.75, 0.73 ± 0.81, and 0.63 ± 0.56 for highly, moderately, and not-mitotoxic PROTACs, respectively. Hence, the morphological difference between mitotoxic and non-mitotoxic PROTACs indicated by higher grit scores is more pronounced at concentrations of 1 and 10 μM. Similar trends were observed for the non-PROTAC compounds (Figure 4a). For example, at concentration 1 μM, the mean grit scores were 2.36 ± 0.88, 1.36 ± 1.34, and 1.04 ± 1.34 for highly, moderately, and not-mitotoxic non-PROTAC compounds, respectively. A UMAP dimensionality reduction was performed on the morphological feature space, which revealed a separation of mitotoxic compounds from not-mitotoxic compounds for both PROTACs and non-PROTACs. Again, this was more evident for the concentrations of 10 and 1 μM (Figure 4b–d). In addition, we observed a similar signature between the PROTACs active on mitochondria and small molecules that showed mitochondrial toxicity such as enclomiphene and amiodarone, suggesting a similar mode of action (Figure 3). In summary, our results indicate that mitotoxic compounds induce distinct phenotypic changes, which are picked up by the Cell Painting assay and which might be used to differentiate between mitotoxic and non-mitotoxic compounds.

The other main observation was that the activity of a PROTAC compound did not always correlate with the activity of the individual PROTAC components. As described above, PROTACs are bifunctional molecules containing a binder for the target of interest and a binder for an E3 ligase, with the two attached together via a linker; most of the PROTACs developed at present use the CRBN or VHL E3 ligases. Binders of CRBN include the clinically approved immunomodulatory drugs (IMiDs) like lenalidomide and pomalidomide. These two IMiD drugs showed no activity in the Cell Painting assay (Table 1 and Figure 2). However, we did at times observe activity of PROTACs even though the primary target

https://doi.org/10.1021/acschembio.2c00076
ACS Chem. Biol. 2022, 17, 1733−1744

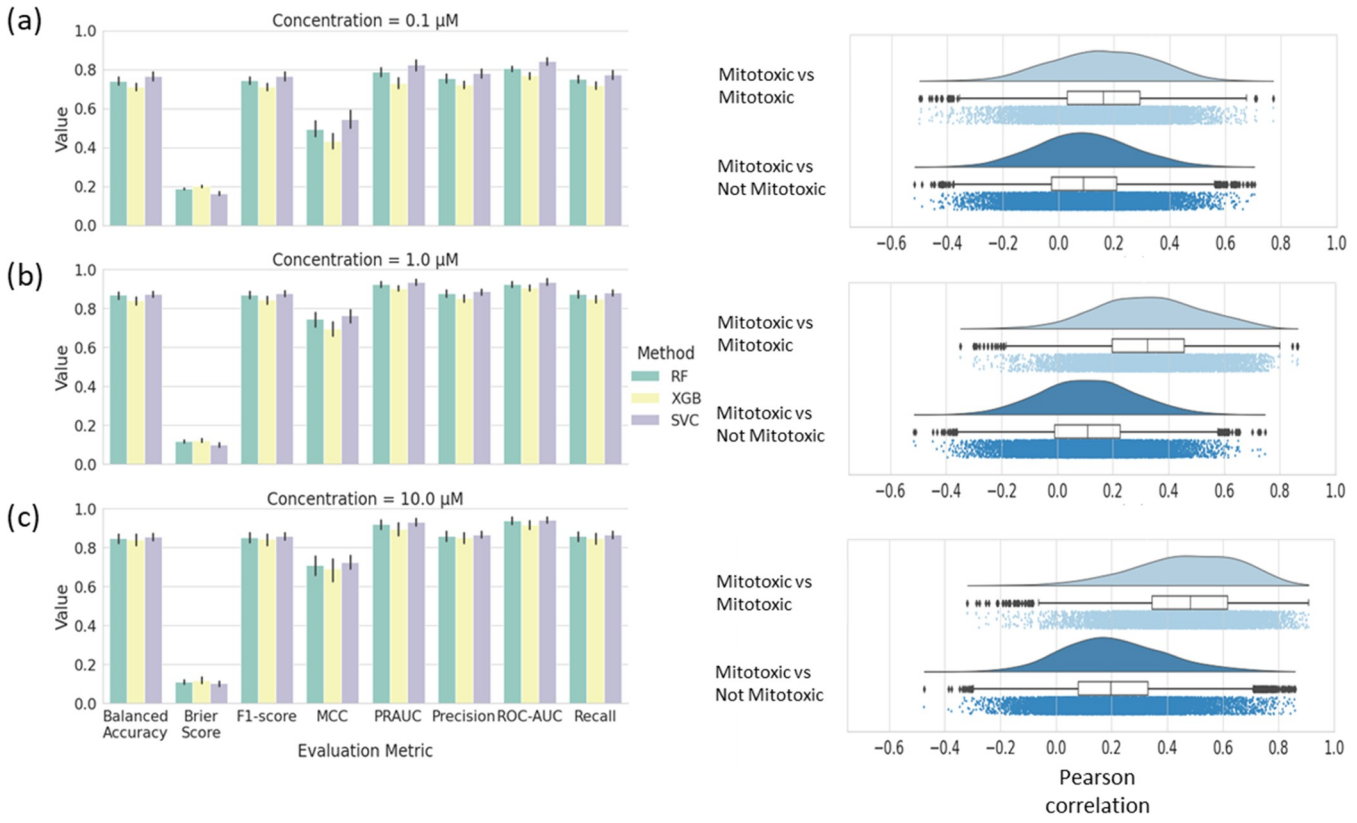

Figure 6. Performance of models for mitochondrial toxicity prediction. Mitochondrial toxicity prediction performance using the Cell Painting features and three different algorithms: RF, XGB, and SVC at concentrations (a) 10, (b) 1, and (c) 0.1 μM. The error bars correspond to the confidence interval across all splits and random states used for cross-validation. Intraclass (mitotoxic vs mitotoxic) vs interclass (mitotoxic vs not mitotoxic) Pearson's correlations of the image-based features are shown for each concentration.

was not expressed in U-2 OS cells like for Target 2, and no activity was observed with the corresponding E3 binder (warhead), binder to the target protein (POI, protein of interest), or known small-molecule inhibitors of the primary target (Figure S4a). Hence, this observation illustrated that PROTAC activity can be more than simply the sum of its parts. Interestingly, modification of the full PROTAC molecule did result in a reduction in Cell Painting activity that was associated with a reduction in mitotoxicity as reported in the Glu/Gal assay considering the full dose response, suggesting that Cell Painting could be used to drive structure−activity relationships (Figure S4a, S4b).

There could be several mechanisms leading to toxicity on mitochondria, direct or indirect. Indirectly, it has been described that accumulation of compounds in lysosomes can lead to mitotoxicity, and lysosomotropic compounds have been shown in previous studies to share similar profiles in phenotypic assays including the Cell Painting assay.[25−27] In addition to protonation and trapping in lysosomes, cationic amphiphilic drugs can cause phospholipidosis and may accumulate in mitochondria, thus leading to mitotoxicity. We therefore investigated what type of mitotoxicity could have been identified in our Cell Painting study. According to the literature, we identified compounds with phospholipidosis activity that showed a dose−response activity in Cell Painting and were active in the Glu/Gal assay (Figures 5a and S5). Interestingly, we also identified compounds with no phospholipidosis activity but still active in the Glu/Gal and Cell Painting assays (Figures 5a and S5). Furthermore, we showed that these compounds caused a direct inhibition of mitochondrial respiration, as seen in a Seahorse experiment testing basal and maximal respiration (Figure 5b), suggesting that two different mitotoxicity mechanisms have been identified in the Cell Painting assay. Looking at the UMAP analysis, the phospholipidosis active compounds clustered together with compounds active in the Glu/Gal assay (Figure 5c). However, it was not clear whether they represent a subcluster group, and more compounds would need to be tested to understand whether Cell Painting can differentiate the mitotoxic signature with different mechanisms (Figure 5c).

Machine Learning Models Showed Good Prediction of Mitochondrial Toxicity. To investigate whether the Cell Painting profiles can be used as descriptors for *in silico* Machine Learning models for mitochondrial toxicity prediction, the profiles were used to train models with three different algorithms, namely, random forest (RF), support vector classifier (SVC), and eXtreme Gradient Boosting (XGB). Models performed very similarly across performance metrics with not one outperforming the other based on multiple metrics (Figure 6). Model performance examples are discussed below using receiver operating characteristic−area under the curve (ROC-AUC) and F1-score (weighted between the two classes) metrics, which are two widely used metrics, and the former shows the ability of the classifier to distinguish between the two classes, whereas the latter considers a model's precision, recalls, and the class imbalance in the model. For example, models showed good predictive performances with ROC-AUC values of 0.80, 0.93, and 0.93 (above 0.80) and F_1-scores of 0.74, 0.87, and 0.85 (above 0.70) for concentrations of 0.1, 1, and 10 μM, respectively, when RF was used (Figure

https://doi.org/10.1021/acschembio.2c00076
ACS Chem. Biol. 2022, 17, 1733−1744

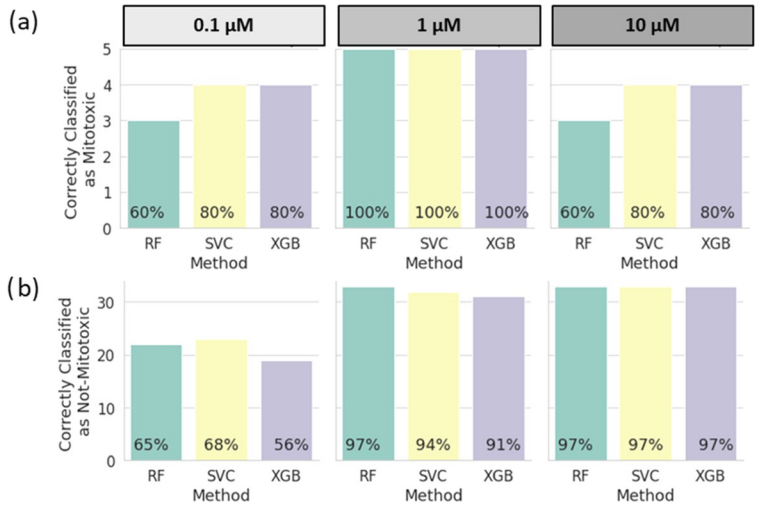

(c)

Compound Number	Grit Score at 0.1μM	Grit Score at 1μM	Grit Score at 10μM	Gal IC50 (μM)
AZ14181856	0.368417	1.187579	2.966919	8.4
AZ14185321	0.596297	2.84736	4.831725	0.077
AZ14185494	0.474734	3.196933	2.32216	0.083
AZ14185492	1.66655	2.088096	2.801327	0.12
AZ14196635	1.284246	0.994007	4.71668	3.6
AZ14170059	0.991725	0.406645	1.06536	>100
AZ14169487	1.174142	0.680144	1.005841	>100
AZ14169488	1.205178	0.414704	0.68391	>100
AZ14169489	-0.31003	-0.13873	1.202298	>100
AZ14169492	0.448893	0.570095	1.174762	>100

Figure 7. Prospective experimental model validation. Number (and percentage) of correctly classified (a) mitotoxic and (b) not-mitotoxic PROTACs, obtained with the models trained with RF, SVC, and XGB algorithms and with data from concentrations 0.1, 1, and 10 μM. (c) Glu/Gal IC_{50} obtained for 10 compounds from the model validation.

6a−c). Similarly, a high performance was achieved by the other two algorithms used, with ROC-AUC and F1-score values being above 0.80 and 0.70, respectively. For example, using the SVC algorithm, the ROC-AUC values were equal to 0.82, 0.93, and 0.95 and the F_1-scores were equal to 0.77, 0.88, and 0.87 when the models were trained with profiles from concentrations 0.1, 1, and 10 μM, respectively (Figure 6a−c). Therefore, the two main observations are that the models perform well (as shown in Figure 6 and the two examples mentioned above) and the models trained with Cell Painting profiles from the two higher concentrations of 1 and 10 μM outperformed the models trained on profiles from the concentration of 0.1 μM.

Concentrations of 1 and 10 μM outperformed the concentration of 0.1 μM regardless of the algorithm used, as shown in Figure 6. This is in agreement with the finding described above: grit scores were larger for mitotoxic compounds at the two higher concentrations than at the lower concentrations tested. Furthermore, this can be explained by the fact that a high intraclass correlation was observed between the mitotoxic compounds in the Cell Painting features at concentrations of 10 and 1 μM with median values of 0.48 and 0.32, respectively, compared to a lower intraclass Pearson correlation at a concentration of 0.1 μM with a median of 0.16 (Figure 6a−d). Hence, PROTACs and compounds that cause mitochondrial toxicity are significantly more similar to each other at concentrations 1 and 10 μM (Figure 6b−d), compared to features derived at 0.1 μM (Figure 6a). Furthermore, a high difference in the intraclass and interclass correlations (between mitotoxic and not mitotoxic) were observed and were equal to 0.07, 0.21, and 0.28 for concentrations 0.1, 1, and 10 μM, respectively. Overall, this means that active compounds at concentrations 10 and 1 μM are clearly different from inactive compounds (median similarities of 0.48 vs 0.20 and 0.32 vs 0.11, respectively) while being less distinguishable at concentration 0.1 μM (median similarities of 0.16 vs 0.09). Taken together, this similarity analysis additionally explains why using concentrations of 1 and 10 μM outperform the model performance at a concentration of 0.1 μM.

Finally, to further validate that the performance is not random, we evaluated whether the models perform better than random models by applying y-scrambling. The y-scrambled models scored mean ROC-AUC values across all algorithms equal to 0.50, 0.51, and 0.49 for concentrations 0.1, 1, and 10 μM, respectively (i.e., close to the expected value of 0.5), as shown in Figure S6a. Hence, the models perform significantly better than the y-scrambling models, and thus, they are unlikely to have been obtained by chance.

Prospective Experimental Model Validation. To further validate our findings, we performed external validation for our mitochondrial toxicity models. Out of the total PROTACs and compounds tested with in the Glu/Gal assay, there were 39 PROTACs that were tested later, out of which five were mitotoxic and 34 were not mitotoxic, which were used as a prospective test set. A similarity analysis (by calculating the Pearson correlation) was initially performed between the 39 query PROTACs to the compounds that cause mitochondrial toxicity and those that do not (i.e., the compounds in the models). For concentrations 1 and 10 μM, the mitotoxic query PROTACs show a higher correlation with the mitotoxic compared to the correlation with the not mitotoxic (Figure S6b). In addition, the not-mitotoxic query PROTACs do not show a high correlation with the mitotoxic PROTACs in the models (Figure S6b). This supported our assumption that the models would be able to also classify the prospective test set correctly.

The mitochondrial toxicity of the 39 PROTACs was hence predicted by all of the models, and the external validation results are summarized in Figure 7a. In addition, results are summarized with confusion matrices and model evaluation metrics in Figure S7. The models trained with data at concentrations 1 and 10 μM performed well and outperformed the models trained with data at a concentration of 0.1 μM (Figure S7a). For example, the balanced accuracies were equal to 0.68, 0.96, and 0.89 when the models were trained with profiles from concentrations 0.1, 1, and 10 μM, respectively (Figure S7b). Moreover, the models trained with the data at a concentration of 0.1 μM showed a relatively high retrieval for mitotoxic PROTACs (more than 60% of mitotoxic PROTACs were correctly classified) (Figure 7a) but, on the other hand,

https://doi.org/10.1021/acschembio.2c00076
ACS Chem. Biol. 2022, 17, 1733−1744

showed high false-positive rates (Figure S7). The models trained with the data from concentrations 1 and 10 μM were consistently able to predict the majority of the mitotoxic PROTACs (Figure 7a), with the models using data from the concentration of 1 μM being able to predict 100% of the mitotoxic PROTACs, regardless of the algorithm used. Models trained with the data from the highest concentration of 10 μM are able to correctly detect 60, 80, and 80% of the mitotoxic PROTACs using the RF, SVC, and XGBOOST algorithms, respectively (Figure 7a). On the other hand, the models trained with data from concentration 10 μM have a lower number of false-positives and thus a higher number of true-negatives compared to models trained with data from concentration 1 μM (Figure S7). Of the not-mitotoxic PROTACs, 97 and 91−97% are correctly classified using the models trained with data from concentrations 10 and 1 μM, respectively (Figures 7b and S7). Considering specific compounds, we confirmed that five compounds that were predicted to be mitotoxic by Cell Painting showed high potency in the Glu/Gal assay (Figure 7c). Interestingly, the grit score also showed a good correlation with the IC_{50} reported in the Glu/Gal (Figure 7c). In contrast, considering five compounds predicted to be mitotoxic inactive, none showed activity in the Glu/Gal assay (Figure 7c). In summary, results from the previous section and this section showed the ability of Cell Painting to correctly and accurately predict mitotoxicity. However, it remains to be established whether the predictive performance levels observed in this study are sufficiently accurate for the pharmaceutical industry to incorporate the system in decision-making in practice.

CONCLUSIONS

The increasing interest in PROTAC as a novel therapeutic modality results in the need for assays to profile these bRo5 compounds (compounds residing just outside of the traditional small-molecule drug physicochemical property space). Therefore, in this work, the Cell Painting assay was used to profile a series of PROTAC and non-PROTAC compounds from various projects based on the hypothesis that the Cell Painting assay could quantitatively study the morphological impact of PROTACs. Two different metrics, a Euclidean distance-based metric and the grit score, revealed that profiles of PROTACs and non-PROTACs are different from the neutral controls, and thus, the Cell Painting assay was able to capture morphological changes induced by PROTACs. In addition, the Euclidean distance-based method and the grit score revealed a higher number of active compounds on the Cell Painting assay and a stronger phenotypic effect, respectively, as the concentration of compounds was increasing.

Focusing on particular examples from published PROTACs, we found that PROTACs degrading targets such as BRD4 show an activity on the Cell Painting assay. In addition, a PROTAC targeting CDK9 (THAL-SNS-032) showed a high activity, and considering the raw images, the phenotype that was observed was consistent with the function of CDK9 in cell-cycle progression. More surprisingly, we observed that the activity of a PROTAC on the Cell Painting assay did not necessarily correlate with the activity of its individual components (i.e., the POI ligand and the E3 ligase ligand). This observation highlighted that PROTACs' activity on the Cell Painting assay is not just the sum of its parts. Furthermore, upon a dimensionality reduction of the PROTACs-Cell Painting profiles with UMAP, we were able to understand whether and which phenotypic responses are clustered together given the target they degrade. Results suggested a range of different and distinguishable Cell Painting signatures for PROTACs targeting various targets such as the BRD4. Considering specific compounds targeting BRD4, the small-molecule inhibitor MS402 clustered together with BRD4 targeting PROTACs, suggesting a similar mode of action. It is difficult at this stage to draw a firm conclusion on the lack of a correlation between primary pharmacology and the grit score generated by Cell Painting. There are many possibilities on why a disconnect can be seen. First, the degradation assays are different for each project, are run in different cell lines, and are based on different technologies. Some assays measure degradation of the endogenous target, and others use target overexpression. Thus, the degradation potency values (pIC_{50}) are not comparable between different targets and, thus, would probably not show a correlation.

However, there were cases where PROTACs showed a Cell Painting activity even though the primary target was not expressed in U-2 OS cells and no activity was observed with the corresponding binder to the target protein. This was an indication that this effect could be related to PROTACs' off-target effect and thus could be useful information to better understand PROTACs' safety profiles. Therefore, we trained *in silico* machine learning models to predict compounds' (including PROTACs) mitochondrial toxicity using the Cell Painting profiles as descriptors for random forest, support vector classifier, and XGB algorithms. Models trained with the Cell Painting features at concentrations 1 and 10 μM outperformed the performance at 0.1 μM. In addition, prospective validation of a model was performed, showing that models trained with data at concentrations 1 and 10 μM performed well. Mitochondrial toxicity is a major safety concern associated with serious organ toxicities and is a frequent cause of late-stage drug withdrawals. With the growing presence of new modalities, including PROTACs, there is an urgent need to evaluate such safety risks for novel compounds. Numerous efforts exist to evaluate or predict small molecule's mitochondrial toxicity, and different assays have been developed capturing various mechanisms of drug-induced mitochondrial toxicity including the Glu/Gal assay used here.[28] However, Hynes et al.[29] showed that the Glu/Gal assay detects only about 2−5% of all mitotoxicants, which further highlights the reality that most compounds that cause organ toxicity do so via multiple off-target mechanisms. Our study highlighted the potential of Cell Painting for mitotoxicity prediction and, given its throughput, could become a very useful method to screen compounds at scale, including new modalities such as PROTACs.

METHODS

Cell Culture and Seeding. U-2 OS cells, a human osteosarcoma cell line, were sourced from AstraZeneca's Global Cell Bank (ATCC Cat# HTB-96). Cells were cultured in McCoy's 5A media (Gibco, #26600023) supplemented with 10% (v/v) fetal bovine serum (Gibco, #10270106) at 37 °C, 5% (v/v) CO_2, 95% humidity. After reaching *ca.* 80% confluency, cells were washed with PBS (Gibco, #10010056) and then detached from culture flasks using the TrypLE Express enzyme (Gibco, #12604013) and resuspended in McCoy's media. Cells were counted using a Vi-CELL (Beckman Coulter, #383556) and then diluted with McCoy's media to achieve a count of 1250 cells per well using a dispense volume of 40 μL per well. The cell suspension was dispensed into CellCarrier-384 Ultra microplates (Perkin Elmer, #6057300) using a Multidrop Combi (ThermoFisher,

https://doi.org/10.1021/acschembio.2c00076
ACS Chem. Biol. 2022, 17, 1733−1744

#5840300) with a standard-tube cassette (ThermoFisher, #24072670). Microplates were left at room temperature for 1 h before transferring to a SteriStore (HighRes Biosolutions) microplate incubator at 37 °C, 5% (v/v) CO_2, 95% humidity for 24 h prior to compound addition.

Compound Treatment. PROTACs were sourced internally through the AstraZeneca Compound Management Group. PROTACs were prepared as 10, 1, and 0.1 μM source stocks (in DMSO) and plated into intermediate 384-well echo-qualified source plates (Labcyte, #PP-0200). After 24 h of seeding, assay plates were dosed using an Echo 655T acoustic dispenser (Labcyte) from the appropriate compound stock to perform a 1000-fold dilution, to achieve assay concentrations of 10, 1, and 0.1 μM. Where required, assay wells had DMSO added to maintain a final DMSO concentration of 0.1% (v/v). Assay plates were returned to the SteriStore incubator for a further 48 h prior to performing the cell staining protocol.

Cell Staining. The Cell Painting staining procedure was performed according to the protocol by Bray et al.[30] with some adjustments to stain concentrations and methodology. Hanks' balanced salt solution (HBSS) 10× was sourced from AstraZeneca's media preparation department and diluted in dH2O and then filtered using a 0.22 μm filter (Corning, CLS430517). MitoTracker stain (ThermoFisher, M22426) was prepared as a 1 mM stock solution in DMSO and then made up as a working stain solution in McCoy's 5A medium, at a final concentration of 0.5 μM. The remaining stains were prepared in 1% (w/v) bovine serum albumin (BSA) (Sigma-Aldrich, A4503) in 1× HBSS containing 0.1% (v/v) Triton X-100 (Sigma-Aldrich, T8787).

Following compound incubation, 10 μL of MitoTracker working solution was added to the plate and incubated for 30 min at 37 °C, 5% CO_2, 95% humidity. The following steps were all carried out at room temperature in the dark. Cells were fixed by adding 25 μL of 12% v/v formaldehyde in PBS (to achieve a final concentration of 3.25% v/v). Plates were incubated for 20 min and then washed using a BlueWasher centrifugal plate washer (BlueCat Bio, Neudrossenfeld, Germany). Following this, 15 μL of stain solution containing 5 μg/mL Hoechst 33342 (ThermoFisher, H3570), 1.5 μg/mL Wheat-germ Agglutinin Alexa Fluor 555 conjugate (ThermoFisher, W32464), 10 μg/mL ConcanavalinA Alexa Fluor 488 conjugate (ThermoFisher, C11252), 5 μL/mL Phalloidin Alexa Fluor 568 conjugate (ThermoFisher, A12380), and 9 μM SYTO14 (ThermoFisher, S7576) was dispensed to each well and incubated for 30 min and then removed prior to a final wash and subsequent addition of 1× HBSS to each well. Plates were sealed and then imaged.

Imaging. Cells were imaged with a CellVoyager CV8000 (Yokogawa, Tokyo, Japan) using a 20× water-immersion objective lens (Olympus, Tokyo, Japan; NA 1.0). Five imaging channels were acquired to visualize all fluorescent stains: DNA (ex: 405 nm; em: 445/45 nm), ER (ex: 488 nm; em: 525/50 nm), RNA (ex: 488 nm; em: 600/37 nm), AGP (ex: 561 nm; em: 600/37 nm), and Mito (ex: 640 nm; em: 676/29 nm). Four fields of view were acquired per well to capture sufficient numbers of cells per perturbation.

Image Analysis and Feature Extraction. Images were saved as 16-bit.tif files without binning (1994 × 1994 pixels). Images were analyzed using CellProfiler biological image analysis software (v 4.0.7). The segmentation of individual nuclei was performed using the DNA channel and subsequent cellular segmentation using the AGP channel. Cells touching the boundary of the image were excluded from subsequent analysis. A total of 4700 features were calculated, relating to either whole-image-level properties or individual objects (cells, nuclei, or cytoplasm). Features include pixel intensity colocalization measurements; granularity and textural measurements of objects taken across a range of pixel distances; the presence and proximity of neighboring objects; the distribution of staining intensity patterns; and size/shape metrics.

Data Curation and Normalization. A normalization process was applied as described by Way et al.[31] First, single-cell data per well were merged by calculating their median value. Next, data were normalized using the median and the median absolute deviation (MAD) of feature values from empty wells (DMSO) as the center and scale parameters, respectively. We normalized all perturbation profiles by subtracting the center (median) and dividing by the scale (MAD) and did this for each plate individually.

Feature Selection. A feature selection was performed to remove features based on a set of criteria. The first criterion was the variance of the features across profiles, and hence, features with a variance less than 1 were removed. In addition, features with a high standard deviation were filtered out, and we used a standard deviation threshold equal to 20. According to Way et al.,[31] features with a high standard deviation after normalization are considered feature outliers and should be removed. In addition, features with missing values in any profile were filtered out. Moreover, pairwise correlations were calculated for all of the features and one feature was randomly removed from each pair with a Pearson correlation greater than or equal to 0.9. As a result of these processes, 669 features remained.

Evaluation of PROTAC Activity on the Cell Painting Assay. Two different methodologies were used to evaluate whether PROTACs were active on the Cell Painting assay screen. The first one was a Euclidean distance-based approach, and the second was the calculation of the grit score. The first approach was described by Cox et al.,[15] and we used it to calculate which PROTACs were "active" on the assay using a 95th percentile cutoff on the null distribution of Euclidean distances between individual DMSO control profiles and the mean DMSO control profile.

In addition, we used the grit score[32,33] (https://github.com/cytomining/cytominer-eval, https://github.com/broadinstitute/grit-benchmark), which captures the phenotypic strength of a perturbation in a profiling experiment and combines two concepts. The first is the replicate reproducibility, and the second is the difference from the DMSO control. First, for each target profile (i.e., PROTACs), pairwise Pearson correlations were calculated for both PROTAC replicates and control replicates. Hence, the pairwise correlations form two distinct distributions (replicate and control). Then, using the control profiles only, a Z-score transform is obtained, which is then used to transform the PROTACs' replicates. The mean of PROTAC replicates' Z-scores is calculated, and this is the final score termed the grit score. Since grit is based on Z-scores, the magnitude can be easily compared between perturbations and is a directly interpretable value. For example, a grit score of 3 for a PROTAC X compared to a neutral control means that on average PROTAC X is 3 standard deviations more similar to replicates than to DMSO controls. Therefore, it is considered the PROTACs' average reproducibility with respect to the neutral control similarity. The grit score was calculated with the cytominer-eval Python package (https://github.com/cytomining/cytominer-eval), developed by the Broad Institute.

Glu/Gal Assay for Mitochondrial Toxicity Assessment. This assay is used to assess potential test substances that can trigger mitochondrial dysfunction. HepG2 cells are cultured in (a) glucose-containing and (b) galactose-containing media and are exposed for 24 h to a concentration of x of the test compounds. Following treatment, the IC_{50} (μM) galactose is measured, and it corresponds to the average galactose signal value, which is halfway between the baseline and the average maximal signal for the substance tested. If IC_{50} (μM) galactose is more than 10, then the substance is considered inactive (i.e., does not cause mitochondrial toxicity), and if it is less than or equal to 10, then it is active and causes mitochondrial toxicity. This mitochondrial toxicity annotation was used to train predictive models for PROTACS' mitochondrial toxicity prediction. In total, 221 compounds (PROTAC and non-PROTAC) were used to train the models with 96 active (mitotoxic) compounds and 125 inactive (not mitotoxic) compounds. Out of the total of 221 compounds, 149 were PROTACs, and in more detail, 90 PROTACs were mitotoxic, with the rest of the PROTACs being not mitotoxic.

Mitochondrial Respiration Assay. HEPG2 C3A cells were cultured in DMEM (Life Technologies) supplemented with 10 Mm galactose (Sigma) and 10% fetal calf serum and seeded onto XFe96 Seahorse Cell Culture microplates at 60,000 cells/well. Cells were cultured overnight in a 37 °C, 5% CO_2 humidified incubator. The following day, the XFe96 sensor cartridge was activated according to

https://doi.org/10.1021/acschembio.2c00076
ACS Chem. Biol. 2022, 17, 1733−1744

the manufacturer's instructions (Agilent), and cells were switched into Agilent Seahorse assay media (DMEM pH 7.4 supplemented with 2 mM glutamine (Agilent) and 10 mM galactose) in a 37 °C incubator for 1 h. PROTAC compounds were prepared in the Seahorse assay media and added to cells immediately prior to the loading of the XFe96 Seahorse cell culture microplate into the Agilent Seahorse XFe96 analyzer. Oligomycin, FCCP, and antimycin were added at 2.5, 2, and 10 μM, respectively, to look at the different stages of mitochondrial respiration.

Phospholipidosis Assay. We used a 2D HepG2 (C3A) hepatoxicity assay to analyze a range of parameters related to cytotoxicity, phospholipidosis, and mitochondrial toxicity. Compound effects are quantified using high-content imaging after the addition of a cocktail of four fluorescent probes (1 μg/mL Hoescht 33342, 6 μg/mL NBD-PE, 50 nM TMRM, and 1 μM TOTO-3) and read on the CellInsight high-content imaging platform.

Mitochondrial Toxicity *In Silico* Model Training and Evaluation. Three times nested fivefold cross-validation was performed with the StratifiedShuffleSplit Python function from Scikit-Learn.[34] The Stratified Shuffle Split (SSS) splits a data set into a train and a test set by preserving the same percentage of data for each class (active and inactive) as in the initial data set. A schematic representation of the model training process is shown in Figure S8.

Initial data were split into 70% train set and 30% test set, respectively, five times using the stratified shuffle split function from Scikit-Learn. The training set was further split five times using the stratified shuffle split function from Scikit-Learn to identify the optimal hyperparameters using the hyperopt and cross-validation score function from Scikit-Learn. When hyperparameters were selected, the models were trained and the compounds in the test set were predicted. This process was repeated with three different random seeds when the initial data was split.

Machine Learning models to predict PROTACs' mitochondrial toxicity were trained with three different algorithms: (a) random forest (RF), support vector classifier (SVC), and (c) XGBOOST (Chen and Guestrin, 2016). RF and SVC were implemented with the RandomForestClassifier and SupportVectorClassifier functions, respectively, from Scikit-Learn[34] and eXtreme Gradient Boosting (XGB) with the XGBClassifier from the xgboost python package.[35] Hyperparameter selection for each of the algorithms was performed using the hyperopt python package.[36,37] The parameters and the range of values (configuration space) that were explored for each algorithm are included in the Supporting Information (Table S1). Cell Painting features were used as descriptors for the models. We used model evaluation metrics from Scikit-Learn, which were averaged to give the overall performance across the different folds of cross-validation for the receiver operating characteristic−area under the curve (ROC-AUC), precision (eq 1), recall (eq 2), F_1-score (eq 3), balanced accuracy (eq 4), the Brier score (eq 5), and the Mathews correlation coefficient (MCC, eq 6).

$$\text{Precision} = \frac{\text{TP}}{\text{TP} + \text{FP}} \tag{1}$$

$$\text{Recall} = \frac{\text{TP}}{\text{TP} + \text{FN}} \tag{2}$$

$$F_1 - \text{score} = 2 \times \frac{\text{Precision} \times \text{Recall}}{\text{Precision} + \text{Recall}} \tag{3}$$

$$\text{Balanced Accuracy} = \frac{\left(\frac{\text{TP}}{\text{TP} + \text{FN}} + \frac{\text{TN}}{\text{FP} + \text{TN}}\right)}{2} \tag{4}$$

$$\text{Brier Score} = \frac{1}{N} \sum_{\text{true value}=1}^{N} (\text{predicted probability} - \text{true value})^2 \tag{5}$$

$$\text{MCC} = \frac{\text{TP} \times \text{TN} - \text{FP} \times \text{FN}}{\sqrt{(\text{TP} + \text{FP})(\text{TP} + \text{FN})(\text{TN} + \text{FP})(\text{TN} + \text{FN})}} \tag{6}$$

TP denotes true-positives, FP denotes false-positives, TN denotes true-negatives, and FN denotes false-negatives.

Finally, y-scrambling[38] was performed to evaluate whether the trained models performed better than the y-scrambled models. Y-scrambling was applied by randomly reorganizing the mitochondrial toxicity labels. Models were rebuilt and evaluated with the same parameters as the unscrambled (actual) models.

Prospective Model Validation. PROTACs that were tested on the mitochondrial toxicity assay after the PROTACs that were included in the benchmarking of models were extracted and used as a prospective validation set. This set included five PROTACs that caused mitochondrial toxicity and 34 PROTACs that did not.

■ ASSOCIATED CONTENT

Supporting Information

The Supporting Information is available free of charge at https://pubs.acs.org/doi/10.1021/acschembio.2c00076.

Figure 1, structure of published PROTAC and non-PROTAC compounds; Figure 2, Pearson's correlation of PROTAC at different concentrations; Figure 3, correlation Cell Painting activity versus primary target degradation; Figure 4, Cell Painting activity for individual PROTAC components; Figure 5, correlation Cell Painting activity versus mitotoxicity and phospholipidosis; Figure 6, performance of y-scrambled models and pairwise Pearson's correlation; Figure 7, prospective experimental model validation results visualized with confusion matrices and model performance on the prospective validation set; Figure 8, schematic representation of the model training process; and Table 1, considered machine learning hyperparameters (PDF)

■ AUTHOR INFORMATION

Corresponding Author

Kevin Moreau − *Safety Innovation, Clinical Pharmacology and Safety Sciences R&D, AstraZeneca, Cambridge CB2 0AA, U.K.*; orcid.org/0000-0002-3688-3998; Email: kevin.moreau@astrazeneca.com

Authors

Maria-Anna Trapotsi − *Department of Chemistry, Centre for Molecular Informatics, University of Cambridge, Cambridge CB2 1EW, U.K.; Data Sciences & Quantitative Biology, Discovery Sciences, BioPharmaceuticals R&D, AstraZeneca, Cambridge CB2 0AA, U.K.*

Elizabeth Mouchet − *High Throughput Screening, Discovery Sciences, BioPharmaceuticals R&D, AstraZeneca, Macclesfield SK10 4TF, U.K.*

Guy Williams − *High Throughput Screening, Discovery Sciences, BioPharmaceuticals R&D, AstraZeneca, Macclesfield SK10 4TF, U.K.*

Tiziana Monteverde − *High Throughput Screening, Discovery Sciences, BioPharmaceuticals R&D, AstraZeneca, Macclesfield SK10 4TF, U.K.*

Karolina Juhani − *High Throughput Screening, Discovery Sciences, BioPharmaceuticals R&D, AstraZeneca, Macclesfield SK10 4TF, U.K.*

Riku Turkki − *Data Sciences & Quantitative Biology, Discovery Sciences, BioPharmaceuticals R&D, AstraZeneca, Gothenburg SE-43183, Sweden*

Filip Miljković − *Imaging and Data Analytics, Clinical Pharmacology & Safety Sciences R&D, AstraZeneca, Gothenburg SE-43183, Sweden;* orcid.org/0000-0001-5365-505X

Anton Martinsson − *Imaging and Data Analytics, Clinical Pharmacology & Safety Sciences R&D, AstraZeneca, Gothenburg SE-43183, Sweden*

Lewis Mervin − *Molecular AI, Discovery Sciences, BioPharmaceuticals R&D, AstraZeneca, Cambridge CB2 0AA, U.K.;* orcid.org/0000-0002-7271-0824

Kenneth R. Pryde − *Oncology Safety, Clinical Pharmacology and Safety Sciences R&D, AstraZeneca, Cambridge CB2 0AA, U.K.*

Erik Müllers − *Bioscience Cardiovascular, Research and Early Development, Cardiovascular, Renal and Metabolism, BioPharmaceuticals R&D, AstraZeneca, Gothenburg SE-43183, Sweden*

Ian Barrett − *Data Sciences & Quantitative Biology, Discovery Sciences, BioPharmaceuticals R&D, AstraZeneca, Cambridge CB2 0AA, U.K.*

Ola Engkvist − *Molecular AI, Discovery Sciences, BioPharmaceuticals R&D, AstraZeneca, Gothenburg SE-43183, Sweden;* orcid.org/0000-0003-4970-6461

Andreas Bender − *Department of Chemistry, Centre for Molecular Informatics, University of Cambridge, Cambridge CB2 1EW, U.K.;* orcid.org/0000-0002-6683-7546

Complete contact information is available at: https://pubs.acs.org/10.1021/acschembio.2c00076

Author Contributions

Conceptualization: E.M., E.M., K.M. Methodology: M.-A.T., E.M., G.W., K.R.P., T.M, R.T., F.M., A.M., L.M. Biological research: E.M., G.W., K.J., T.M. Data analysis: G.W, K.M., M.-A.T. Writing: K.M, E.M., M.-A.T. Supervision: K.M., A.B., I.B., O.E., L.M. All authors discussed the results and commented on the manuscript.

Notes

The authors declare the following competing financial interest(s): All the authors are employees of AstraZeneca except of Trapotsi MA and Bender A.

■ ACKNOWLEDGMENTS

The authors thank their AstraZeneca colleagues for the internal reviewing and the helpful discussion during the preparation of the manuscript. M.-A.T. thanks the Biotechnology and Biological Sciences Research Council (BBSRC) [BB/M011194/1] and AstraZeneca for funding.

■ REFERENCES

(1) Ermondi, G.; Garcia-Jimenez, D.; Caron, G. Protacs and Building Blocks: The 2d Chemical Space in Very Early Drug Discovery. *Molecules* **2021**, *26*, 672.

(2) Lipinski, C. A.; Lombardo, F.; Dominy, B. W.; Feeney, P. J. Experimental and Computational Approaches to Estimate Solubility and Permeability in Drug Discovery and Development Settings. *Adv. Drug Delivery Rev.* **1997**, *23*, 3−25.

(3) Zhao, P.; Peng, Y.; Xu, X.; Wang, Z.; Wu, Z.; Li, W.; Tang, Y.; Liu, G. In Silico Prediction of Mitochondrial Toxicity of Chemicals Using Machine Learning Methods. *J. Appl. Toxicol.* **2021**, *41*, 1518−1526.

(4) Hemmerich, J.; Troger, F.; Füzi, B.; F Ecker, G. Using Machine Learning Methods and Structural Alerts for Prediction of Mitochondrial Toxicity. *Mol. Info.* **2020**, *39*, No. 2000005.

(5) Zhang, H.; Chen, Q. Y.; Xiang, M. L.; Ma, C. Y.; Huang, Q.; Yang, S. Y. In Silico Prediction of Mitochondrial Toxicity by Using GA-CG-SVM Approach. *Toxicol. In Vitro* **2009**, *23*, 134−140.

(6) Moreau, K.; Coen, M.; Zhang, A. X.; Pachl, F.; Castaldi, M. P.; Dahl, G.; Boyd, H.; Scott, C.; Newham, P. Proteolysis-Targeting Chimeras in Drug Development: A Safety Perspective. *Br. J. Pharmacol.* **2020**, *177*, 1709−1718.

(7) Trapotsi, M.; Barrett, I.; Engkvist, O.; Bender, A. Bioinformatic Approaches in the Understanding of Mechanism of Action (MoA). In *Target Discovery and Validation*; Plowright, A. T., Ed., 2020 DOI: 10.1002/9783527818242.ch11.

(8) Trapotsi, M. A.; Mervin, L. H.; Afzal, A. M.; Sturm, N.; Engkvist, O.; Barrett, I. P.; Bender, A. Comparison of Chemical Structure and Cell Morphology Information for Multitask Bioactivity Predictions. *J. Chem. Inf. Model.* **2021**, *61*, 1444−1456.

(9) Gustafsdottir, S. M.; Ljosa, V.; Sokolnicki, K. L.; Anthony Wilson, J.; Walpita, D.; Kemp, M. M.; Petri Seiler, K.; Carrel, H. A.; Golub, T. R.; Schreiber, S. L.; et al. Multiplex Cytological Profiling Assay to Measure Diverse Cellular States. *PLoS One* **2013**, *8*, No. e80999.

(10) Hofmarcher, M.; Rumetshofer, E.; Clevert, D. A.; Hochreiter, S.; Klambauer, G. Accurate Prediction of Biological Assays with High-Throughput Microscopy Images and Convolutional Networks. *J. Chem. Inf. Model.* **2019**, *59*, 1163−1171.

(11) Simm, J.; Klambauer, G.; Arany, A.; Steijaert, M.; Wegner, J. K.; Gustin, E.; Chupakhin, V.; Chong, Y. T.; Vialard, J.; Buijnsters, P.; et al. Repurposing High-Throughput Image Assays Enables Biological Activity Prediction for Drug Discovery. *Cell Chem. Biol.* **2018**, *25*, 611−618.e3.

(12) Young, D. W.; Bender, A.; Hoyt, J.; McWhinnie, E.; Chirn, G. W.; Tao, C. Y.; Tallarico, J. A.; Labow, M.; Jenkins, J. L.; Mitchison, T. J.; Feng, Y. Integrating High-Content Screening and Ligand-Target Prediction to Identify Mechanism of Action. *Nat. Chem. Biol.* **2008**, *4*, 59−68.

(13) Seal, S.; Yang, H.; Vollmers, L.; Bender, A. Comparison of Cellular Morphological Descriptors and Molecular Fingerprints for the Prediction of Cytotoxicity- And Proliferation-Related Assays. *Chem. Res. Toxicol.* **2021**, *34*, 422−437.

(14) Martin, H. L.; Adams, M.; Higgins, J.; Bond, J.; Morrison, E. E.; Bell, S. M.; Warriner, S.; Nelson, A.; Tomlinson, D. C. High-Content, High-Throughput Screening for the Identification of Cytotoxic Compounds Based on Cell Morphology and Cell Proliferation Markers. *PLoS One* **2014**, *9*, No. e88338.

(15) Cox, M. J.; Jaensch, S.; Van de Waeter, J.; Cougnaud, L.; Seynaeve, D.; Benalla, S.; Koo, S. J.; Van Den Wyngaert, I.; Neefs, J. M.; Malkov, D.; et al. Tales of 1,008 Small Molecules: Phenomic Profiling through Live-Cell Imaging in a Panel of Reporter Cell Lines. *Sci. Rep.* **2020**, *10*, No. 13262.

(16) Nyffeler, J.; Willis, C.; Lougee, R.; Richard, A.; Paul-Friedman, K.; Harrill, J. A. Bioactivity Screening of Environmental Chemicals Using Imaging-Based High-Throughput Phenotypic Profiling. *Toxicol. Appl. Pharmacol.* **2020**, *389*, No. 114876.

(17) Bray, M.-A.; Gustafsdottir, S. M.; Rohban, M. H.; Singh, S.; Ljosa, V.; Sokolnicki, K. L.; Bittker, J. A.; Bodycombe, N. E.; Dančík, V.; Hasaka, T. P.; et al. A Dataset of Images and Morphological Profiles of 30 000 Small-Molecule Treatments Using the Cell Painting Assay. *GigaScience* **2017**, *6*, No. giw014.

(18) Chandrasekaran, S. N.; Ceulemans, H.; Boyd, J. D.; Carpenter, A. E. Image-Based Profiling for Drug Discovery: Due for a Machine-Learning Upgrade? *Nat. Rev. Drug Discovery* **2021**, *20*, 145−159.

(19) Trapotsi, M.-A.; Hosseini-Gerami, L.; Bender, A. Computational Analyses of Mechanism of Action (MoA): Data, Methods and Integration. *RSC Chem. Biol.* **2022**, *3*, 170−200.

(20) Dykens, J. A.; Will, Y. The Significance of Mitochondrial Toxicity Testing in Drug Development. *Drug Discovery Today* **2007**, *12*, 777−785.

(21) Olson, C. M.; Jiang, B.; Erb, M. A.; Liang, Y.; Doctor, Z. M.; Zhang, Z.; Zhang, T.; Kwiatkowski, N.; Boukhali, M.; Green, J. L.;

et al. Pharmacological Perturbation of CDK9 Using Selective CDK9 Inhibition or Degradation. *Nat. Chem. Biol.* **2018**, *14*, 163−170.
(22) Carotenuto, P.; Pecoraro, A.; Palma, G.; Russo, G.; Russo, A. Therapeutic Approaches Targeting Nucleolus in Cancer. *Cells* **2019**, *8*, 1090.
(23) McInnes, L.; Healy, J.; Melville, J. UMAP: Uniform Manifold Approximation and Projection for Dimension Reduction, arXiv.1802.03426. arXiv.org e-Print archive. https://doi.org/10.48550/arXiv.1802.034262018.
(24) Rana, P.; Aleo, M. D.; Gosink, M.; Will, Y. Evaluation of in Vitro Mitochondrial Toxicity Assays and Physicochemical Properties for Prediction of Organ Toxicity Using 228 Pharmaceutical Drugs. *Chem. Res. Toxicol.* **2019**, *32*, 156−167.
(25) Schneidewind, T.; Brause, A.; Schölermann, B.; Sievers, S.; Pahl, A.; Sankar, M. G.; Winzker, M.; Janning, P.; Kumar, K.; Ziegler, S.; Waldmann, H. Combined Morphological and Proteome Profiling Reveals Target-Independent Impairment of Cholesterol Homeostasis. *Cell Chem. Biol.* **2021**, *28*, 1780−1794.e5.
(26) Laraia, L.; Garivet, G.; Foley, D. J.; Kaiser, N.; Müller, S.; Zinken, S.; Pinkert, T.; Wilke, J.; Corkery, D.; Pahl, A.; et al. Image-Based Morphological Profiling Identifies a Lysosomotropic, Iron-Sequestering Autophagy Inhibitor. *Angew. Chem., Int. Ed.* **2020**, *59*, 5721−5729.
(27) Lu, S.; Sung, T.; Lin, N.; Abraham, R. T.; Jessen, B. A. Lysosomal Adaptation: How Cells Respond to Lysosomotropic Compounds. *PLoS One* **2017**, *12*, No. e0173771.
(28) Will, Y.; Dykens, J. Mitochondrial Toxicity Assessment in Industry − a Decade of Technology Development and Insight. *Expert Opin. Drug Metab. Toxicol.* **2014**, *10*, 1061−1067.
(29) Hynes, J.; Nadanaciva, S.; Swiss, R.; Carey, C.; Kirwan, S.; Will, Y. A High-Throughput Dual Parameter Assay for Assessing Drug-Induced Mitochondrial Dysfunction Provides Additional Predictivity over Two Established Mitochondrial Toxicity Assays. *Toxicol. In Vitro* **2013**, *27*, 560−569.
(30) Bray, M.-A.; Singh, S.; Han, H.; Davis, C. T.; Borgeson, B.; Hartland, C.; Kost-Alimova, M.; Gustafsdottir, S. M.; Gibson, C. C.; Carpenter, A. E. Cell Painting, a High-Content Image-Based Assay for Morphological Profiling Using Multiplexed Fluorescent Dyes. *Nat. Protoc.* **2016**, *11*, 1757−1774.
(31) Way, G. P.; Kost-Alimova, M.; Shibue, T.; Harrington, W. F.; Gill, S.; Piccioni, F.; Becker, T.; Shafqat-Abbasi, H.; Hahn, W. C.; Carpenter, A. E.; Vazquez, F.; Singh, S. Predicting Cell Health Phenotypes Using Image-Based Morphology Profiling. *Mol. Biol. Cell* **2021**, *32*, 995−1005.
(32) GitHub. cytomining/cytominer-eval: Common Evaluation Metrics for DataFrames. https://github.com/cytomining/cytominer-eval (accessed Oct 25, 2021).
(33) GitHub. broadinstitute/grit-benchmark: Benchmarking a metric used to evaluate a perturbation strength. https://github.com/broadinstitute/grit-benchmark (accessed Oct 25, 2021).
(34) Pedregosa, F.; Varoquaux, G.; Gramfort, A.; Michel, V.; Thirion, B.; Blondel, M. G. O.; Prettenhofer, P.; Weiss, R.; D, V. Scikit-Learn: Machine Learning in Python. *J. Mach. Learn. Res.* **2011**, *12*, 2825−2830.
(35) Chen, T.; Guestrin, C. *XGBoost: A Scalable Tree Boosting System*, Proceedings of the 22nd ACM SIGKDD International Conference on Knowledge Discovery and Data Mining, 2016; pp 785−794 DOI: 10.1145/2939672.2939785.
(36) Bergstra, J.; Yamins, D.; Cox, D. *Making a Science of Model Search: Hyperparameter Optimization in Hundreds of Dimensions for Vision Architectures*, Proceedings of the 30th International Conference on Machine Learning, 2013; pp 115−123. PMLR February 13.
(37) Bergstra, J.; Komer, B.; Eliasmith, C.; Yamins, D.; Cox, D. D. Hyperopt: A Python Library for Model Selection and Hyperparameter Optimization. *Comput. Sci. Discovery* **2015**, *8*, No. 014008.
(38) Lipiński, P. F. J.; Szurmak, P. SCRAMBLE'N'GAMBLE: A Tool for Fast and Facile Generation of Random Data for Statistical Evaluation of QSAR Models. *Chem. Pap.* **2017**, *71*, 2217−2232.

https://doi.org/10.1021/acschembio.2c00076
ACS Chem. Biol. 2022, 17, 1733−1744